IOP Publishing Metrologia
Metrologia **49** (2012) 70–81 doi:10.1088/0026-1394/49/1/011

# Report on the first international comparison of small force facilities: a pilot study at the micronewton level

**Min-Seok Kim[1], Jon R Pratt[2], Uwe Brand[3] and Christopher W Jones[4]**

[1] Korea Research Institute of Standards and Science (KRISS), Daejeon, Republic of Korea
[2] National Institute of Standards and Technology (NIST), Gaithersburg, MD, USA
[3] Physikalisch-Technische Bundesanstalt (PTB), Braunschweig, Germany
[4] National Physical Laboratory (NPL), Hampton Road, Teddington, Middlesex, TW11 0LW, UK

E-mail: jon.pratt@nist.gov

Received 2 August 2011, in final form 27 September 2011
Published 28 November 2011
Online at stacks.iop.org/Met/49/70

**Abstract**
Measurements of forces less than a micronewton are critical when examining the mechanical behaviour of materials and devices at characteristic length scales below a micrometre. As a result, specification standards for nanomechanical tests and test equipment are being proposed by international standards organizations, and an infrastructure for traceable small force calibration is developing. In this context, results are reported from the first interlaboratory comparison of micronewton-level force metrology. The basis of the comparison was the calibration of a set of five piezoresistive cantilever force sensors similar to those used for atomic force microscopes but employed here as transfer artefacts. The artefacts were circulated among four national metrology institutes with each using their own force balance to calibrate the stiffness (force change per unit displacement) and sensitivity (signal output change per unit force) of the artefacts. By considering the weighted mean of the stiffness and sensitivity values reported for a given artefact, reference values were obtained. The largest contributing uncertainty components were due to the transfer artefacts themselves, rather than from the measurements of the physical quantities of force, voltage and displacement. The results imply that it should be possible to determine cantilever stiffness using force balance techniques with an accuracy of better than 1% if necessary, but that improvements in the ability to orient the transfer artefacts, to characterize the non-linearity of their output, and to compensate for the stiffness of the associated fixtures and load frames are required if the resolution of future comparisons is to improve.

(Some figures may appear in colour only in the online journal)

## 1. Introduction

In the last decade, a number of national metrology institutes (NMIs) worldwide have worked to extend the range of traceable force measurement down to the nanonewton level, in response to increasing demands for traceable micro- to nanonewton force metrology from dependent industries and academic groups [1–6]. Each of these NMIs has built a small force facility or developed artefacts based on individual designs and operating principles [7–10], and studied the dissemination of the resultant traceable micronewton force realization through diverse paths. Examples include the direct stiffness calibration of various micro-scale cantilevers used in atomic force microscopy (AFM) with a small force facility [11, 12]; the use of calibrated transfer artefacts specifically devised for *in situ* calibration of AFM cantilevers [13–19]; and the use of a conductive probe to apply traceable electrical forces either directly to instrumented indentation sensors [20] or to AFM colloidal probes [21, 22].

The potential uncertainties in the calibration of small force sensors or artefacts using the developed small force facilities have been estimated and reported [7, 12]. The results

  

of calibration with small force facilities have been used as a cross-check in assessing the accuracy of other stiffness calibration methods either via direct comparisons [16, 21–24] or indirectly, through a piezoresistive transfer artefact (that is, a cantilever equipped with piezoresistive deflection sensing metrology) [18, 25].

The calibration uncertainties of each of these small force facilities, including both primary realization and dissemination routes, have been estimated by the respective NMI. An additional level of verification through inter-laboratory comparisons seems, at first glance, unnecessary, since all were derived from traceable measurement practices. However, whenever a variety of artefacts and methods emerge that purport to calibrate the same measurand, obvious questions concerning the degree of equivalence arise that can only be addressed by direct comparison. Furthermore, such comparisons are the only means to reveal otherwise unknowable sources of uncertainty, such as systematic errors from physical effects not otherwise accounted for. Consequently, the comparison of a diversity of instruments, and methodologies is the only way to ensure that validated measurement techniques can be developed for use as the basis of an international standard. In macro-scale force metrology, for example, NMIs that maintain deadweight force standard machines (or other types of force standard machines) as a primary force standard participate in International Committee for Weights and Measures (CIPM) intercomparisons organized by the relevant Consultative Committee or by the Regional Metrology Organizations. Highly stable force transducers are circulated among the participants and the results of calibration are compared with a reference value (RV). Differences in the reported values and the corresponding estimated calibration uncertainties determine the degree of equivalence of national metrology services. Through such comparisons, the calibration and measurement capabilities (CMCs) of NMIs are verified and permitted to be mutually recognized under the CIPM mutual recognition arrangement (MRA).

Anticipating that the needs of science and commerce for the creation, production and testing of so-called micro- and nanotechnologies will evolve along paths similar to that of macro-scale antecedents, a formal demonstration of equivalence as described above will soon be necessary for micro-scale force metrology. This perception motivates the comparison work that is the focus of this paper. Because small force standards are still in a nascent stage, this first international comparison on force at micronewton levels was necessarily organized as an informal pilot study among NMIs who have developed small force standards. The comparison was co-piloted by the Korea Research Institute of Standards and Science (KRISS) and the National Institute of Standards and Technology (NIST), and included the National Physical Laboratory (NPL) and the Physikalisch-Technische Bundesanstalt (PTB).

The primary realizations of force used in this pilot study can be divided into two types: electrical force-based methods and mass-based methods. The NIST and NPL facilities realize traceable forces based on the electrostatic compensation of external forces under the electrostatic force balance (EFB) principle; force traceability is derived from the definition of the metre and the electrical units of capacitance and voltage under the International System of Units (SI). In contrast, the PTB and KRISS primary standards are realized based on conventional deadweight principles using high-precision mass comparators. In this scheme, force traceability is achieved by calibrating mass comparators with small, calibrated weights.

As may be expected, calibration procedures employed for micro-force metrology are not yet standardized, and the methods employed in this study deviate from those used in macro-force metrology, such as the standardized procedures described in the standard ISO 376 [26]. It was decided by consensus that, rather than adhering to existing macro-force protocols, the participants would create a loose protocol of their own that would have enough flexibility to allow all to participate with a minimum of modifications to their facilities. Specifically, the participants agreed that the comparison would focus on the measurement of the spring constant and the force sensitivity for each of a set of five piezoresistive cantilevers. Such devices are available commercially and are similar to the type of cantilever force sensor that has been studied previously at each institute. Briefly, the comparison was carried out as follows. NIST supplied five commercial micro-force sensors of a piezoresistive cantilever type along with a mounting fixture and corresponding bridge amplifier. These sensors, the mounting fixture and the bridge amplifier served as the transfer artefacts. KRISS prepared a general guide and a brief protocol. The transfer artefacts were circulated among participants from February 2008 to January 2010. During this period, each participant measured the spring constants and force sensitivities of the transfer artefacts using small forces, procedures and data-processing methods specific to their unique facilities. In the following sections, the small force facilities and transfer artefacts are described in greater detail; the general calibration procedures including the protocols, data-processing and uncertainty evaluation methods are also described. Finally the comparison results are presented and discussed.

## 2. Small force facilities

The small force facilities used in this comparison each employ precision balances to measure or generate an SI-traceable force with a resolution of better than 1 nN. The facilities mainly differ in the approaches employed for traceable force realization, and hence the type of balance used. The method employed by KRISS and PTB uses a precision commercial ‘mass comparator’ (a mass balance) that has a resolution of 0.1 µg (corresponding to approximately 1 nN). The mass comparator operates in a force-compensation mode. When an unknown external force is applied to the mass comparator, an electromagnetic force generated by a coil and a permanent magnet in the mass comparator counteracts the external force so as to maintain a constant balance position. The balance electromagnetic force scale is compared with a traceable mass scale by weighing calibrated masses ranging from 0.05 mg to 100 mg on the balance [12]. The known mass scale is converted to force through knowledge of the gravitational acceleration at

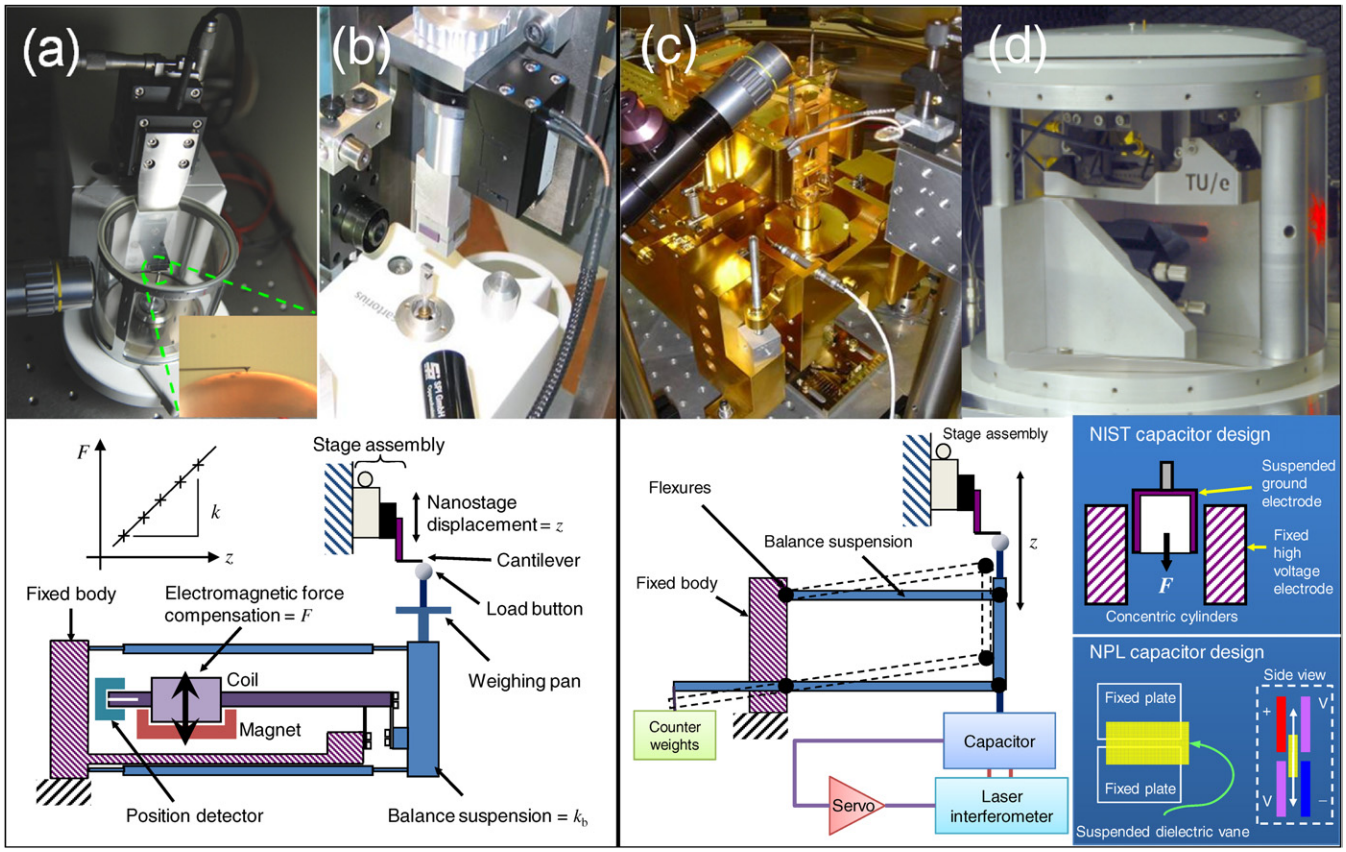


**Figure 1.** Low-force facilities used in this work and their schematic diagrams illustrating their operations: small force standards traceable to the SI unit of mass at (*a*) KRISS and (*b*) PTB; small force standards based on electrical units of SI at (*c*) NIST and (*d*) NPL.

the balance location. In other words, the unknown external forces are compared indirectly with the traceable deadweights via the balance's electromagnetic forces.

The other method, employed by NIST and NPL, is an electrostatic force-based approach that achieves force traceability from the SI units of length, capacitance and voltage. This electrostatic method incorporates a force balance consisting of a capacitor that generates calculable electrostatic forces, a uniaxial (four-bar) flexure system that constrains the motion of the moving capacitor component to a path parallel to the vertical axis of the balance and a laser interferometer that measures the displacement of that moving capacitor component. In general, an electrostatic force $F_e$ is generated in the capacitor when a voltage is applied across the capacitor. For a two-electrode capacitor, the electrostatic balance principle gives the force $F_z$ generated along the balance axis $z$ as

$$F_e = F_z = \frac{1}{2}\frac{dC}{dz} \cdot V^2 \qquad (1)$$

where $V$ is the voltage across the capacitor pair and $C$ its capacitance. The capacitance gradient $dC/dz$ can be linearized with the appropriate choice of capacitor design. The NIST design uses nested concentric cylinders, with one cylinder constrained to move coaxially within the other. The NPL design uses a moving dielectric sheet partially inserted between four fixed capacitor plates.

Figure 1 illustrates the facilities of the participants and summarizes their principles of operation. More detailed descriptions of the instruments are given elsewhere [7, 10, 27] (KRISS, PTB and NIST). Similarly, the concept and operation scheme of the NPL low force balance (LFB) were previously reported in [8, 28]; however, revisions due to repair and optimization have resulted in a slightly different force generation principle that is outlined here.

The LFB contains a monolithic flexure mechanism with inherent alignment of the uniaxial vertical motion applied to the attached dielectric vane. This vertical motion is monitored via a differential plane mirror interferometer, which has an effective deadpath of the order of 1 mm and as such is largely insensitive to refractive index variation.

The electrostatic drive contains four capacitor plates arranged vertically in two pairs (see figure 1(*d*)). Equal and opposite fixed voltages are supplied to one diagonally opposite pair; a variable voltage is supplied to the remaining plates. The zero-deflection position of the dielectric vane is at the midpoint of the plates; total capacitance is proportional to deflection. The generated force in this design is (to first order) proportional to the fixed voltage, the variable voltage and the linear capacitance gradient over the full force range. This linear variable-voltage dependence, which respects the form of equation (1), significantly simplifies balance controller operation.

All signals are modulated in phase with a 1 kHz carrier that prevents humidity-related surface charge accumulation on the dielectric vane whilst maintaining the instantaneous polarity

relationship required for equation (1) to hold. An amplifier–transformer system produces the final drive voltage, with a range–uncertainty trade-off selectable via the transformer ratio.

## 3. Small force transfer standards

An ideal small force transfer artefact would have a well-defined loading point and a repeatable output, and would be insensitive to off-axis load. Such an artefact would be self-contained, possessing its own sensors for converting the applied load into a usable readout, with the majority of processing electronics onboard. In addition, it would be small enough to fit within the limited space of the target instrument and be robust with respect to environmental changes and other disturbances that might occur during shipping. To date, a small force transfer standard that fulfils all these requirements has not yet been developed [23, 29]. Most small force sensors used for nanomechanical testing have to date adopted a cantilever design as a compromise. The comparison described here used examples of the popular, and commercially available, piezoresistive cantilever force sensor format as small force transfer artefacts despite their drawbacks, which include vulnerability to off-axis load, and parasitic transverse movement of the sensor tip (the loading point) during sensor deflection.

The piezoresistive cantilevers and the accompanying bridge amplifier were obtained commercially from Kleindiek Nanotechnik GmbH[5]. Two sensor models (FMT-400 and FMT-120) with different length and spring constant were available. The FMT-400 model has a length of approximately 400 µm, a maximum force of 80 µN and a spring constant ranging from 2 N m$^{-1}$ to 4 N m$^{-1}$, and the FMT-120 sensor has a length of approximately 120 µm, a maximum force of 360 µN and a spring constant ranging from 30 N m$^{-1}$ to 40 N m$^{-1}$, according to the manufacturer's specification [30]. Three FMT-400 sensors (artefacts #1, #2 and #3) and one FMT-120 sensor (artefact #5) were used in this comparison. The optical microscope image of the sensor shown in figure 2(*a*) reveals that an additional, very short, cantilever is suspended from the same cantilever chip. The piezoresistor on this dummy cantilever forms one arm of a Wheatstone resistance bridge and facilitates compensation for changes in resistance due to temperature variation. A conical-shaped tip is situated at the end of the cantilever and its position forms the contact point between the cantilever and the interacting system.

The installed FMT sensor is held mechanically with a plug-in holder with four spring clips. The cantilever is oriented on the plug-in holder with its tip side facing upwards; the spring clips then form electrical contacts with the piezoresistors and other Wheatstone bridge elements on the sensor chip. The plug-in holder was modified with a threaded stud as shown in figure 2(*b*) to enable installation of the sensor on the participating primary small force balances. The sensor

[5] The identification of any commercial product or trade names does not imply endorsement or recommendation by the National Institute of Standards and Technology.

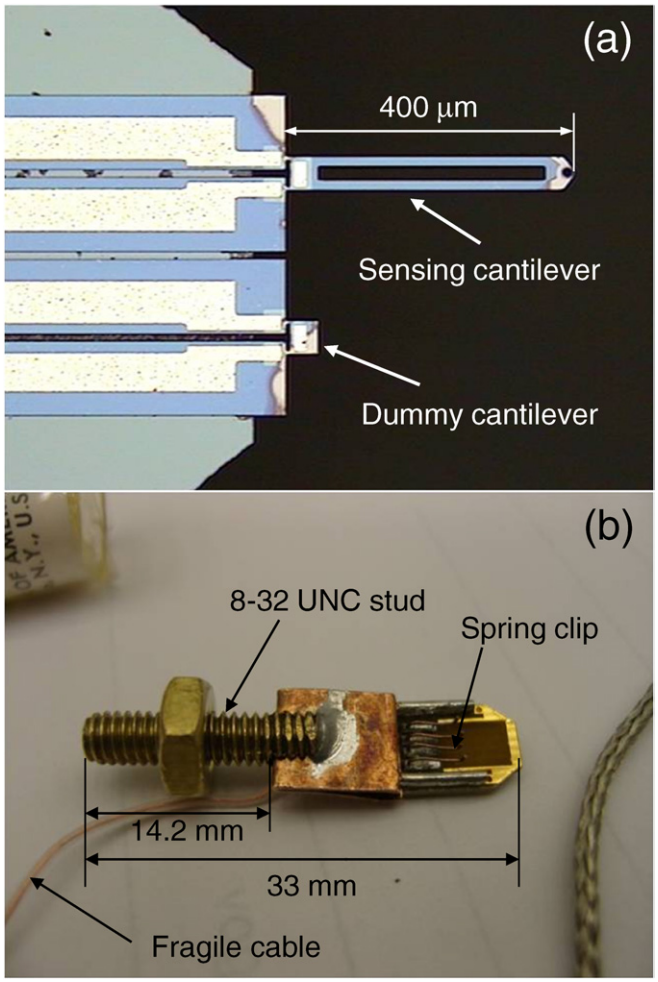


**Figure 2.** Transfer artefact used in this comparison: (*a*) an optical microscope image of the Kleindeik Nanotechnick™ FMT-400 piezoresistive cantilever sensor chip, (*b*) a modified plug-in holder with a threaded stud (Unified Thread Standard, 8-32 UNC).

bridge amplifier produces an output voltage ranging from 0 V to approximately 10 V, proportional to the cantilever's deflection. Beginning with an unloaded cantilever (no force applied to the tip), the sensor output was set to zero using the coarse and fine adjustment controls on the sensor bridge amplifier.

## 4. Calibration of the small force transfer standards

Each participant determined the spring constants $k$ (expressed in units of N m$^{-1}$) and the force sensitivities $S$ (expressed in units of V N$^{-1}$) of the transfer artefacts using their own standards and procedures. The artefact spring constant and force sensitivity were chosen as measurands for the small force comparison since these quantities are also commonly used in AFMs and other nanomechanical testing instruments. The measurement protocol that was circulated among the participants provided only minimal guidance on how to configure and use the Kleindiek equipment and FMT sensors. The common aspects of the calibration setups and procedures, along with those specific to each participant, are considered in the following subsections.

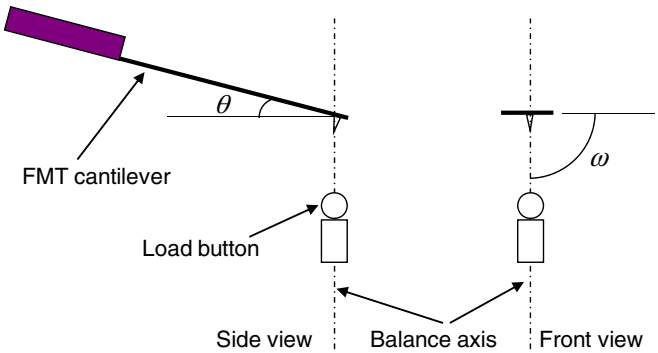


**Figure 3.** Orientation of the FMT sensor axis with respect to the balance axis. The orientation would be best when angles $\theta$ and $\omega$ are 0° and 90°, respectively.

### *4.1. Common experimental details*

The measurement protocol circulated with the transfer artefacts recommended that the FMT sensors be positioned with respect to the various balances so that the plane of the cantilever would be perpendicular to the balance axis as indicated in figure 3. This orientation differs from the usual tilted orientation of an AFM probe and was selected in order to maximize the sensitivity and optimize the alignment of the cantilever bending axis with respect to the direction of the applied force. No method was specified for achieving this orientation and participants performed the alignment by eye. This alignment can be critical, because friction forces between the tip and balance platen can produce spurious torques, or pseudo-forces, if $\theta$ and $\omega$ deviate from 0° and 90°, respectively. The degree to which spurious forces are a factor during calibration is difficult to determine, but is known to depend on the amount of misalignment, along with a number of other variables, including the coefficient of friction, the tip geometry, the cantilever length [12, 31] and the stiffness of the cantilever relative to that of the surface [24]. Rather than attempting to fully characterize alignment-induced pseudo-forces, participants in this comparison agreed to use judgment to place a bound on their magnitude. The assessment of this type B uncertainty is discussed later.

At the start of a calibration, each cantilever was loaded up to the point of maximum measurable deflection, where the voltage output of the amplifier was in the range 9.0 V to 9.9 V, slightly lower than the saturation voltage (around 10.5 V). Calibration scans were executed by subdividing this maximum deflection into four or five evenly distributed loading increments. The force–deflection and force–voltage data were acquired by repeatedly stepping through these load increments, sampling the force, displacement and voltage simultaneously for 10 s to 20 s at each step and averaging them after the balance readings stabilized, which took from 30 s to 70 s. The maximum allowable deflection was determined to be approximately 5 µm for the FMT-400 sensors and approximately 0.6 µm for the FMT-120 sensors used in the reported work. Accordingly, the maximum force was approximately 10 µN for the FMT-400 sensors and 50 µN for FMT-120 sensors. The maximum force recorded during the experiment varied somewhat from one scan to another during the calibration, due to the drift of the balances (thermal, mechanical, etc) and the pseudo-force originating from slight length changes of the measurement loop. Thermal expansion of the components and sliding of the tip along the surface of the load button can extend or shorten the length of the measurement loop [12]. The voltage output of the amplifier was measured using a high-resolution (more than 6.5 digit) voltmeter. In most cases, more than 30 force curves were obtained (except in NPL's experiments, 15 force curves) and processed to determine each spring constant and the corresponding force sensitivity.

Environmental conditions for the measurements were not specified in the protocol in consideration of the different primary force standards adopted among participants; the NIST EFB works in vacuum, whereas the KRISS, NPL and PTB machines operate under ambient conditions. All participants reported that the nominal surrounding temperature was in the range 20 °C to 25 °C. In previous work [7], temperature was observed to have little effect on the spring constant and force sensitivity of a similar sensor, and temperature variation from NMI to NMI was not a factor in this comparison.

### *4.2. Different experimental details among participants*

*4.2.1. Balance scan (indenter mode) against cantilever scan.* NIST employs a balance scan, or indenter mode, to calibrate artefacts. This scheme is illustrated in the lower right inset of figure 1 for the case of an electrostatic balance. Briefly, the force sensor is held in a fixed position by a stage assembly while the balance mechanism is translated using servo-control to make contact with, and then deflect, the cantilever. In contrast, KRISS, PTB and NPL employ a cantilever scan or the balance null-deflection technique to calibrate artefacts. This scheme is illustrated in the lower left inset of figure 1 for the case of a compensation balance. In this case, the base of the FMT sensor is scanned along the $z$-axis of the primary balance using a precision linear stage. After contact is made, and as the cantilever deflects, the balance compensation force acts to hold the position of the balance platen fixed. In either case, the scanning of the stage or the balance is controlled to produce cantilever deflections through the range of steps described previously.

The indentation technique using the EFB has an advantage of being able to measure both the applied force and the resultant cantilever deflection traceably along the same, well-defined line of action. However, as the electrostatic force pushes the platen against the FMT sensor, it includes contributions from the mechanical stiffness and hysteresis of the balance flexure system that must be taken into consideration. The mechanical stiffness of the EFB can be adjusted and was observed to behave as a simple spring having effective stiffness $k_{\mathrm{EFB}}$, which was measured directly by recording force–displacement data while cycling the EFB through an indentation sequence in the absence of a sample. The balance stiffness was obtained by fitting the slope of the resulting force–displacement curves. A set of 30 such non-contact indents were performed immediately before and after testing each FMT sensor, with the average of the slopes before and after

being used to estimate the balance stiffness during the actual calibration test. The measured values for $k_{EFB}$ varied between approximately 0.01 N m$^{-1}$ and 0.03 N m$^{-1}$ over the course of all of the experiments. The mechanical hysteresis observed by analysing the force residuals during these experiments was negligible.

The null-deflection method shared by KRISS, PTB and NPL requires that the length scale incorporated in the precision linear stage be calibrated using traceable dimensional metrology, e.g. a laser interferometer, for the traceable determination of stiffness. Knowledge of the stiffness of the balance $k_B$ is typically not required because each balance operates in an external-load-compensation mode. Theoretically, $k_B$ is infinite; practically, it is high but finite, measured to be approximately 1600 N m$^{-1}$ [7] for the KRISS facility and 11 kN m$^{-1}$ for the PTB facility. These finite values of $k_B$ are mostly due to the different line of action between the compensation force and the external force (see figure 1) in mass balances of electromagnetic force compensation type. A correction is required for $k_B$, but in this case $k_B$ is serially connected to the cantilever spring. Thus, the correction becomes critical only when the spring constant of a stiff artefact is to be determined. In the case of NPL's LFB, these two forces have the same line of action, and $k_B$ is assumed to be high enough (of the order of 0.1 MN m$^{-1}$ to 1 MN m$^{-1}$) to be negligible with respect to the stiffness calibrations of FMT sensors under normal LFB operation and in the work described here.

*4.2.2. Load frame stiffness correction.* Correction is also required for the so-called load frame stiffness, $k_L$, which stems from the finite stiffness of the components, such as the sensor mount and three-axis stage, that comprise a force and measurement loop in the calibration setup. NIST measured $k_L$ directly by probing the EFB against the base of the cantilever. The load frame stiffness was determined to be (2600 ± 500) N m$^{-1}$. On the other hand, KRISS measured $k_L$ directly by placing loads on the upper side of the plug-in holder (i.e. not the base of the cantilever) and measuring its vertical displacements through a calibrated optical microscope; $k_L$ was determined to be approximately (20 000 ± 5000) N m$^{-1}$. NPL did not measure $k_L$ for this work since it is not expected to be a dominant source of uncertainty for the compliant FMT-400 artefact. PTB also measured $k_L$ directly by probing against the base of the cantilever, and it was determined to be (14490 ± 250) N m$^{-1}$. Interestingly, a difference in $k_L$ between loading and unloading conditions was observed during PTB's load frame stiffness measurements. The $k_L$ during loading and unloading was measured to be 13 200 N m$^{-1}$ and 15 770 N m$^{-1}$, respectively. It is suspected that compliance of the plug-in holder accounts for this difference and the big discrepancy among determined values of $k_L$ from NIST and PTB. As shown in figure 2(*b*), the plug-in holder grips the FMT sensor with just four compliant spring clips made of a copper sheet, such that the sensor could be displaced or tilted somewhat during the probing. The load frame stiffness-measuring method of KRISS cannot account for the stiffness between the FMT sensor and the plug-in holder because the load is directly applied to the plug-in holder, not through the base of the cantilever like the NIST and PTB methods. This can contribute to an overall calibration uncertainty, which will be discussed in the next section.

The corrected spring constants $k_C$ were computed from the measured spring constants $k_M$ as

$$\frac{1}{k_C} = \frac{1}{k_M - k_{EFB}} - \frac{1}{k_L} \tag{2a}$$

in the case of NIST's method, and

$$\frac{1}{k_C} = \frac{1}{k_M} - \frac{1}{k_B} - \frac{1}{k_L} \tag{2b}$$

in the case of KRISS's, NPL's and PTB's method. In the case of NIST's method, the force sensitivity $S$ was corrected for the stiffness of the EFB as

$$S = \frac{F_E - k_{EFB} \times z}{V} \tag{3}$$

where $F_E$ is the electrostatic force generated by the coaxial cylinders, $z$ is the displacement and $V$ is the output of the bridge amplifier.

*4.2.3. Force loading directions.* NIST, PTB and NPL applied both ascending and descending forces to calibrate both the spring constant and the force sensitivity. In every cycle, two slopes for each of the quantities were obtained and averaged. Contact between the tip of the cantilever and the balance load button was maintained throughout the series of scans making up the calibration. NIST performed post-processing of the acquired data to compensate for the drift of the balance. At each cycle, the average force and associated timestamp were recorded, and a high-order polynomial was fitted to the complete force–time dataset. Using this polynomial, the drift of force was taken out and the stiffness and the force sensitivity were corrected accordingly. NPL also removed the force drift, which appeared as a constant (zero-order) term in the linear fits of each dataset. PTB applied different $k_L$ values for the correction of measured spring constants $k_M$ in accordance with loading directions when using equation (2*b*).

The KRISS procedure used only ascending forces to determine both quantities, and the contact was broken and remade at every scan, so that the first (zero-load) data point was always acquired while out of contact. The first data point was thus excluded during the linear-fit operation to determine the stiffness correctly. In the case of force sensitivity, the first point was not excluded. KRISS did not perform the post-processing of the data to compensate for the drift of the balance. Instead, the balance scale was zeroed using the manufacturer's tare function before acquiring the first data point at every new scan.

*4.2.4. NPL's participation in this work.* Given the value of continual international cooperation in the micro-force measurement field, NPL's participation is a valuable part of this comparison. It should be noted, however, that the NPL's LFB was not fully optimized for the described work. In particular,

**Table 1.** Summary of calibration results of all transfer artefacts; FMT-400 (#1, #2, #3) and FMT-120 (#5) from KRISS, NIST, PTB and NPL listed in chronological order.

| Date | Institute | Stiffness ± expanded uncertainty $k_c \pm U(k_c)$/N m$^{-1}$ (fractional, %) | Force sensitivity ± expanded uncertainty $S \pm U(S)$/V mN$^{-1}$ (fractional, %) | Loading direction: both (ascending and descending) or single (ascending) | # of force curves | Average temperature /°C |
|---|---|---|---|---|---|---|
| *Transfer artefact #1* | | | | | | |
| 2008-02-11 | KRISS | 2.301 ± 0.031(1.3) | 1028 ± 15(1.5) | Single | 60 | 24.34 |
| 2008-05-05 | NIST | 2.300 ± 0.058(2.5) | 1026 ± 23(2.3) | Both | 179 | 21.0 |
| 2008-10-27 | PTB | 2.295 ± 0.066(2.9) | 1035 ± 30(2.9) | Both | 30 | 20.27 |
| 2009-07-09 | KRISS | 2.307 ± 0.029(1.2) | 1030 ± 15(1.5) | Single | 110 | 22.99 |
| *Transfer artefact #2* | | | | | | |
| 2008-02-20 | KRISS | 1.705 ± 0.027(1.6) | 1315 ± 20(1.5) | Single | 20 | 24.73 |
| 2008-04-17 | NIST | 1.711 ± 0.041(2.4) | 1310 ± 29(2.2) | Both | 202 | 21.1 |
| 2008-09-17 | PTB | 1.684 ± 0.049(2.9) | 1332 ± 38(2.9) | Both | 34 | 20.93 |
| 2009-07-03 | KRISS | 1.712 ± 0.021(1.2) | 1320 ± 17(1.3) | Single | 110 | 22.69 |
| *Transfer artefact #3* | | | | | | |
| 2008-05-23 | NIST | 1.668 ± 0.040(2.5) | 1254 ± 27(2.2) | Both | 44 | 21.1 |
| 2008-09-22 | PTB | 1.662 ± 0.049(2.9) | 1271 ± 36(2.8) | Both | 26 | 20.32 |
| 2008-11-24 | NIST | 1.665 ± 0.040(2.5) | 1255 ± 27(2.2) | Both | 120 | 21.2 |
| 2009-06-25 | KRISS | 1.667 ± 0.020(1.2) | 1261 ± 16(1.3) | Single | 110 | 22.92 |
| 2010-02-28 | NPL (electric) | 1.69 ± 0.21(12.5) | 1234 ± 54(4.4) | Both | 15 | 20.0 |
| | NPL (mass) | 1.65 ± 0.21(12.9) | 1267 ± 54(4.3) | | | |
| *Transfer artefact #5* | | | | | | |
| 2008-02-14 | KRISS | 78.4 ± 2.2(2.8) | 206.2 ± 3.0(1.5) | Single | 76 | 24.51 |
| 2008-05-27 | NIST | 79.2 ± 7.5(9.4) | 205.6 ± 4.4(2.2) | Both | 98 | 21.0 |
| 2008-09-23 | PTB | 76.1 ± 3.03(3.9) | 205.9 ± 8.0(3.9) | Both | 66 | 20.11 |
| 2008-12-10 | NIST | 78.9 ± 7.5(9.4) | 205.0 ± 4.4(2.2) | Both | 212 | 21.1 |
| 2009-07-15 | KRISS | 77.5 ± 2.1(2.8) | 205.4 ± 3.1(1.5) | Single | 110 | 23.37 |

the generated voltages were not measured directly but inferred from a traceable offline calibration of the voltage generation circuitry.

Consequently, uncertainties in raw force readings to be presented from the LFB are significantly higher than it is understood to be possible for the instrument. The discrepancy between electrostatic force and deadweight scales had been observed to be approximately 2.5% at about 30 µN and is not explained by the uncertainty in either route. It should be noted that this discrepancy does not represent the best-case performance of the LFB.

For these reasons, NPL acted as an observer in this comparison, and the NPL-reported values did not contribute to the calculation of the comparison RV. In this capacity, NPL calibrated one FMT-400 sensor (artefact #3) on the LFB. Due to above-mentioned concern about systematic errors limiting the performance of the LFB, NPL decided to report calibrated values calculated via two routes:

(1) electrostatic force traceability: that is, force values traceable through voltage and capacitance gradient measurements, in line with the NIST approach, and
(2) mass traceability: that is, relying only on the scale linearity and proven stability of the LFB force signal, the absolute value of which is calibrated via the comparison with a 'calibrated' mass artefact of approximately 2.9 mg. This scheme is similar to KRISS's and PTB's approach.

A scale factor, $\gamma_F$, was used to calculate the artefact's stiffness and force sensitivity, based on mass traceability, from the raw force readings of the LFB. The scale factor is defined by

$$F_{mass} = \gamma_F F_{el} \tag{4}$$

where $F_{mass}$ and $F_{el}$ are the mass-traceable force and the LFB force, respectively. The scale factor was estimated to be $0.974 \pm 0.010$ ($k = 1$) through weighing experiments on the LFB, which included about 7200 transitions (i.e. mass artefact loading and unloading on the LFB) over six days. The calibration, based on the comparison between the LFB's electrostatic force scale and the SI mass scale, was dominated by systematic uncertainties in the force reading, based on prior characterization of the device. The relative uncertainty in $\gamma_F$, defined by this calibration, was therefore used as a good estimate for the relative uncertainty in a LFB force reading from either traceability route. Due to constraints imposed by the parallel mass traceability operation, the force range–uncertainty trade-off achieved in the LFB 1 kHz calibrated ac voltage supply transformer ratios could not be optimized for the cantilever calibration. These challenges are logistical rather than metrological in nature.

## 5. Comparison results and uncertainties

### *5.1. Calibration results of the stiffness and sensitivity of transfer artefacts*

Table 1 summarizes the results of calibrations of transfer artefacts from all participants, listed in chronological order, including the number of force curves, loading directions, mean

**Table 2.** Uncertainty budget for the spring constants and force sensitivities of the transfer artefacts #3 and #5 from all participants, KRISS, NIST, PTB and NPL. The symbol '—' in the blank means that the uncertainty component was not considered independently for the calculation of overall uncertainty estimation.

| | Artefact #3 (FMT-400 model) | | | | | | | | Artefact #5 (FMT-120 model) | | | | | |
|---|---|---|---|---|---|---|---|---|---|---|---|---|---|---|
| | Spring constant/mN m$^{-1}$ | | | | Force sensitivity/V mN$^{-1}$ | | | | Spring constant/mN m$^{-1}$ | | | Force sensitivity/V mN$^{-1}$ | | |
| Uncertainty source | KRISS | NIST | PTB | NPL | KRISS | NIST | PTB | NPL | KRISS | NIST | PTB | KRISS | NIST | PTB |
| Repeatability | 0.3 | 0.4 | 4.0 | — | 0.1 | 0.24 | 1.5 | — | 0.1 | 0.02 | 0.2 | 0.06 | 0.02 | 0.1 |
| Force | 1.7 | 0.8 | 17.0 | 17 | 1.3 | 0.6 | 12.8 | 13 | 0.0 | 0.0 | 0.8 | 0.02 | 0.00 | 2.1 |
| Displacement | 2.4 | 0.0 | 1.0 | 51 | — | — | — | — | 0.4 | 0.0 | 0.2 | — | — | — |
| Non-linearity | 2.1 | 10.8 | — | 92 | 4.0 | 4.7 | — | 23 | 0.9 | 3.6 | — | 1.04 | 0.73 | — |
| Voltage | — | — | — | — | 0.0 | 0.0 | 0.0 | 1 | — | — | — | 0.00 | 0.00 | 0.00 |
| Stiffness of the measurement loop (balance and load frame) | 0.1 | 0.2 | 0.4 | — | — | — | 0.3 | — | 0.1 | 0.4 | 1.0 | — | — | 2.7 |
| Orientation | 9.3 | 16.7 | 17.0 | 10 | 6.8 | 12.5 | 12.9 | 7 | 0.4 | 0.8 | 0.8 | 1.11 | 2.10 | 2.1 |
| Temperature | | | | | | | | negligible | | | | | | |
| Combined standard uncertainty, $u_c$ | 10.0 | 19.9 | 24.4 | 107 | 8.0 | 13.4 | 18.2 | 27 | 1.1 | 3.7 | 1.5 | 1.5 | 2.2 | 4.0 |
| Result of measurements, $Y \pm U(Y)$, $k = 2$ | $1667 \pm 20$ | $1666 \pm 40$ | $1662 \pm 49$ | $1690 \pm 210$ | $1261 \pm 16$ | $1255 \pm 27$ | $1271 \pm 36$ | $1234 \pm 54$ | $77.9 \pm 2.1$ | $79.0 \pm 7.5$ | $76.1 \pm 3.0$ | $205.7 \pm 3.1$ | $205.3 \pm 4.4$ | $205.9 \pm 8.0$ |

temperature and associated uncertainties. Where possible, all transfer artefacts were recalibrated after returning from a participant, by either KRISS (for artefacts #1, #2 and #5) or NIST (for artefacts #3 and #5), in order to verify their stability during transportation. As seen in table 1, the transfer artefacts did not show significant drift in either stiffness or sensitivity following shipping and transportation. Additionally, no correlation is seen between measured stiffness or sensitivity and the average temperature during calibration. Table 2 shows the uncertainty budget in the estimates of spring constants and force sensitivities of artefacts #3 (representative compliant artefact) and #5 (stiffer artefact) along with the final values from all participating NMIs. In the cases where data were obtained from two separate runs as part of the stability check, the mean of all data was taken as the representative measured value reported by the NMI.

A weighted mean of the participants' results was used as a RV for the comparison. The NPL data were omitted from the determination of the RVs of artefact #3 according to NPL's observer status. Figures 4 and 5 graphically show the measurement results of artefacts #3 and #5 from all participants, respectively. The error bars represent the expanded uncertainty ($k = 2$) intervals of the participants' reported results. Large error bars were allowed to run off the figure to magnify the distribution of the reported values. The blue dashed lines indicate expanded uncertainty bounds on the RVs. For information, the comparison results for artefacts #1 and #2 are shown in figures A1 and A2. It should be noted that all error bars in figures 4, 5, A1 and A2 cross the baseline and the uncertainty bounds of RVs for both stiffness and force sensitivity. Furthermore, reported mean values from KRISS, NIST and PTB are in the uncertainty bounds of RVs. This indicates that the results from all participants agree with the RVs within the uncertainties associated with those results.

Differences among the claimed uncertainties from KRISS, NIST and PTB range approximately from 20 mN m$^{-1}$ to 70 mN m$^{-1}$ for stiffness and from 15 V mN$^{-1}$ to 40 V mN$^{-1}$ for sensitivity for artefact #3, and range from 2 N m$^{-1}$ to 7 N m$^{-1}$ for stiffness and from 3 V mN$^{-1}$ to 9 V mN$^{-1}$ for sensitivity for artefact #5.

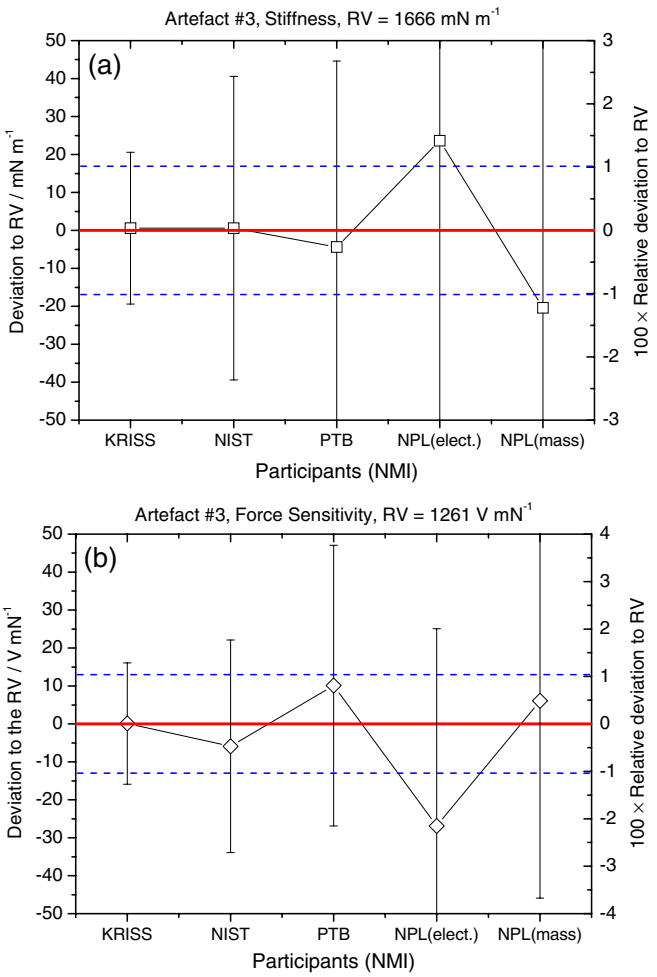


**Figure 4.** Comparison results for (*a*) the stiffness and (*b*) the force sensitivity of artefact #3 after subtraction of the RVs: (*a*) 1666 mN m$^{-1}$ and (*b*) 1261 V mN$^{-1}$ calculated from the weighted mean values of the measurement data. Dashed blue lines represent expanded uncertainties of the RVs. Note that mean values reported from KRISS, NIST and PTB are within the uncertainty bounds of RVs (error bars are described in the text).

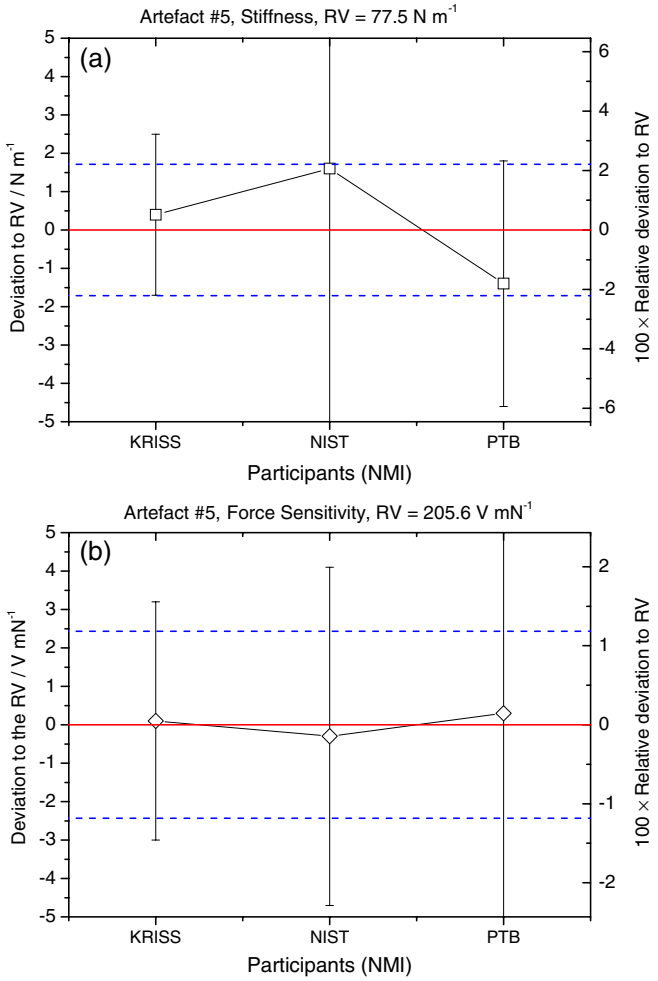


**Figure 5.** Comparison results for (*a*) the stiffness and (*b*) the force sensitivity of artefact #5 after subtraction of the RVs: (*a*) 77.5 N m$^{-1}$ and (*b*) 205.6 V mN$^{-1}$ calculated from weighted mean values of the measurement data. Dashed blue lines represent the expanded uncertainties of the RVs. Note that all reported mean values are within the uncertainty bounds of RVs (error bars are described in the text).

As described previously, the NPL LFB was operated in a non-optimized setup during experiments. Nevertheless, all of NPL's results, calculated via both the mass- and electrostatics-traceability routes, agree with the RVs for both the stiffness and the sensitivity of artefact #3. From figures 4(*a*) and (*b*), it can be seen that NPL's results calculated via the mass-traceable route are closer to RVs than those calculated via the electrostatics-traceable route, suggesting the presence of additional systematic uncertainties associated with indirect measurement of voltage on the LFB.

### 5.2. *Uncertainty estimations of all participants*

Uncertainties were estimated using a protocol loosely based on an approach previously reported by KRISS [12], with each participant making adjustments to the protocol to accommodate unique features of their individual setups. Here, we describe differences in the uncertainty estimation among participants in detail.

The force uncertainty for each participant was estimated in accordance with the specific type of primary force equipment used in the comparison. The force uncertainty for KRISS and PTB is dominated by the uncertainties of standard mass artefacts used for calibration of the mass comparators. In the case of the NIST EFB, the force uncertainty is dominated by the surface potential on the balance electrodes, which was not measured in this series of experiments, but in the past has never exceeded four parts in 10 000. NPL used the uncertainty in $\gamma_F$ as a good estimate of the relative force uncertainty as described in the previous section.

KRISS, PTB and NPL estimated the displacement uncertainty based on the calibration results of the precision moving stages with traceable displacement metrology, such as a laser interferometer, whereas NIST used the laser interferometer directly for deflection measurements of the cantilevers and thus could give the lowest uncertainty among participants.

NIST assessed the non-linearity by calculating two point slopes for all of the individual increments (both approach and retract) and examining the standard deviation of these slopes, whereas KRISS calculated two point slopes for all of the individual increments, classifying slopes into five groups according to which segment of curves they belong to, averaging them for each group and examining the maximum difference among the averaged slopes[6]. NPL examined residuals to the least-squares linear fit to each curve and estimated the non-linearity error as the maximum absolute value among segment slopes of residuals' curves. Those values corresponded to residuals in the calibration of the cantilever scan stage against the LFB internal interferometer. It is suggested that finite cantilever scan stage performance accounts for the majority of the NPL displacement and non-linearity uncertainty estimates, and that better mounting and characterization could produce stiffness uncertainties of 80 mN m$^{-1}$ ($k = 2$). PTB included the non-linearity error of the balance in the force uncertainty contribution, which is estimated to be ±9 nN. The uncertainty associated with voltage measurement was negligible, because all participants used high-precision voltmeters to measure the bridge amplifier output.

The uncertainties in the stiffness correction terms $k_L$ and $k_B$ (see section 4.2.2) are propagated through equations (2*a*) and (2*b*) and contribute to the overall measurement uncertainty for $k_C$. The uncertainty due to incomplete determination of the load frame stiffness, $u_{lf}(k_C)$, can be given by [12]

$$\frac{u_{lf}(k_C)}{k_C} = \frac{1}{\sqrt{3}} \left| \frac{k_M}{k_L - k_M} \right| \frac{\Delta k_L}{k_L} \tag{5}$$

where $\Delta k_L$ is the maximum error in the determination of the load frame stiffness. The uncertainty due to incomplete determination of the balance stiffness can be calculated by just replacing $k_L$ with $k_B$ in equation (5). Each participant estimated the uncertainty due to these stiffnesses differently according to the participant facility's mechanical load structure

[6] Since all force curves have five segments, five averaged slopes are obtained. The averaged slope obtained from first segment slopes was omitted prior to examination since the first data point was acquired without contact in the KRISS experiments.

and mode of operation. In each case, the participants agreed that the uncertainties in the determination of $k_L$ were dominated by the instability and compliance of the mechanical connection between the FMT sensor and the plug-in holder, as described previously. NIST and PTB could directly measure $k_L$ in a fashion that included the stiffness between the FMT sensor and the plug-in holder, whilst KRISS could not. NPL did not measure $k_L$ because the correction itself was estimated to contribute less than 2% to the combined uncertainty when the compliant artefact #3 was calibrated (see table 2). Comparing figures 4(*a*) and 5(*a*), it can be seen that relative deviations of the stiffness values of artefact #5 among three NMIs (KRISS, NIST and PTB) are greater than those of artefact #3. We suspect that unstable stiffness of the load frame and the difference in its correction method among participants might account for this result.

The uncertainty originating from misalignment of the artefact includes a cosine error, associated with the misalignment of the cantilever plane normal relative to the balance axis, and a friction term associated with the interface between the tip of the cantilever and the load button under such misalignment. All participants calculated an uncertainty due to this friction component based on the following equation [12]:

$$\frac{k_\theta}{k_0} = \frac{1}{\cos\theta(\cos\theta - \mu\sin\theta)} \tag{6}$$

where $k_\theta$ and $k_0$ are the measured stiffness at contact angles $\theta$ and 0, respectively, and $\mu$ is the coefficient of static friction. Assuming that the coefficient of friction is less than 0.3 and that the misalignment $\theta$ in figure 3 is bound to $\pm 1^\circ$ (KRISS, NPL) and $\pm 2^\circ$ (NIST, PTB), this friction contribution corresponds to a relative uncertainty of approximately 0.6% and 1%, respectively.

It should be noted that, in general, the largest contributing uncertainty sources are those originating from the transfer artefacts themselves: non-linearity, orientation, stiffness of the measurement loop (arising from the unstable sensor mounting holder discussed earlier), rather than measurements of physical quantities: force, displacement and voltage. This implies that more advanced transfer artefacts are necessary in order to improve the resolution of future comparisons.

## 6. Conclusions

The first interlaboratory comparison of traceable micronewton-level force metrology was conducted as a pilot study among NMIs KRISS, NIST, NPL and PTB from February 2008 to February 2010. Two types of commercial devices, consisting of cantilevers with piezoresistive deflection sensing metrology, were used as transfer artefacts. The medium of comparison was the measurement of the stiffness (force change per unit displacement) and sensitivity (signal output change per unit force) of each of the devices.

This comparison includes various types of primary small force measurement facilities, developed using different traceable force realization principles (mass-based and electrical-force-based approaches) and different designs. The comparison protocol permitted some variation in calibration

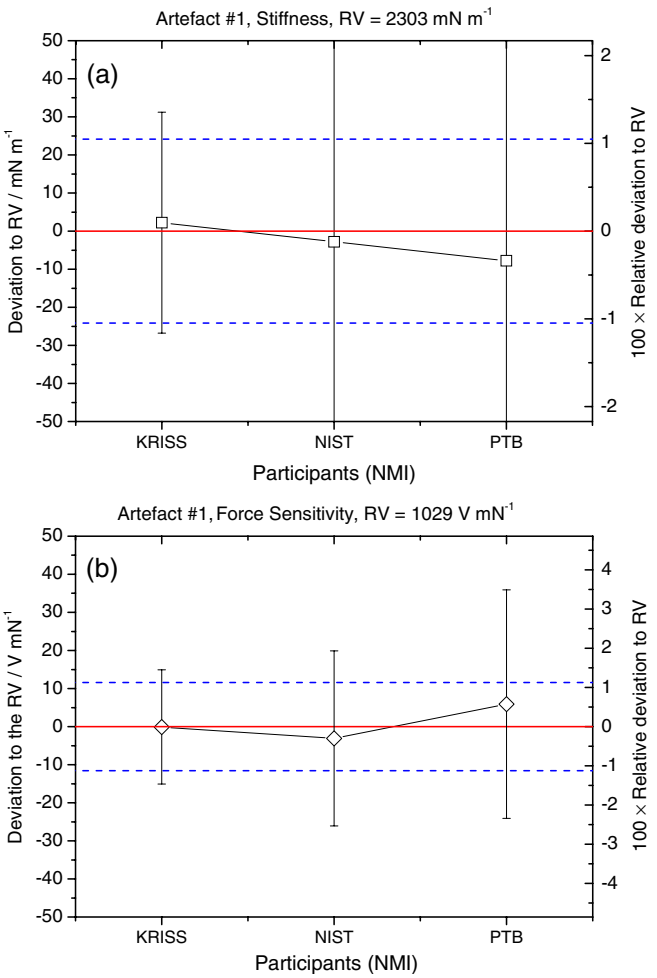


**Figure A1.** Comparison results for (*a*) the stiffness and (*b*) the force sensitivity of artefact #1 after subtraction of the RVs: (*a*) 2303 mN m$^{-1}$ and (*b*) 1029 V mN$^{-1}$ calculated from the weighted mean values of the measurement data. Dashed blue lines represent the expanded uncertainties of the RVs. Note that all reported mean values are within the uncertainty bounds of RVs (error bars are described in the text).

procedures and data-processing methods among participants. Nevertheless, the results of measurements are in good agreement, suggesting that the calibration capabilities of the participating small force facilities are equivalent within their reported uncertainties. Furthermore, based on the comparison results shown in figures 4, 5, A1 and A2, it seems likely that the capability for each participant has been conservatively estimated. Further investigation of the sources of systematic uncertainties and a better choice of transfer artefact are necessary to estimate capabilities more accurately and to improve understanding of the discrepancies in the results of stiffness and sensitivity measurements.

For future comparisons, a more rigorous technical protocol should be developed and adopted. Such a protocol should regulate measurement procedures, data-processing methods and the calculation of uncertainties, including the budget of systematic uncertainties for individual small force facilities in accordance with the GUM [32], and additionally, regulate the presentation of the results. Better transfer artefacts will also be necessary to enhance the level of comparison.

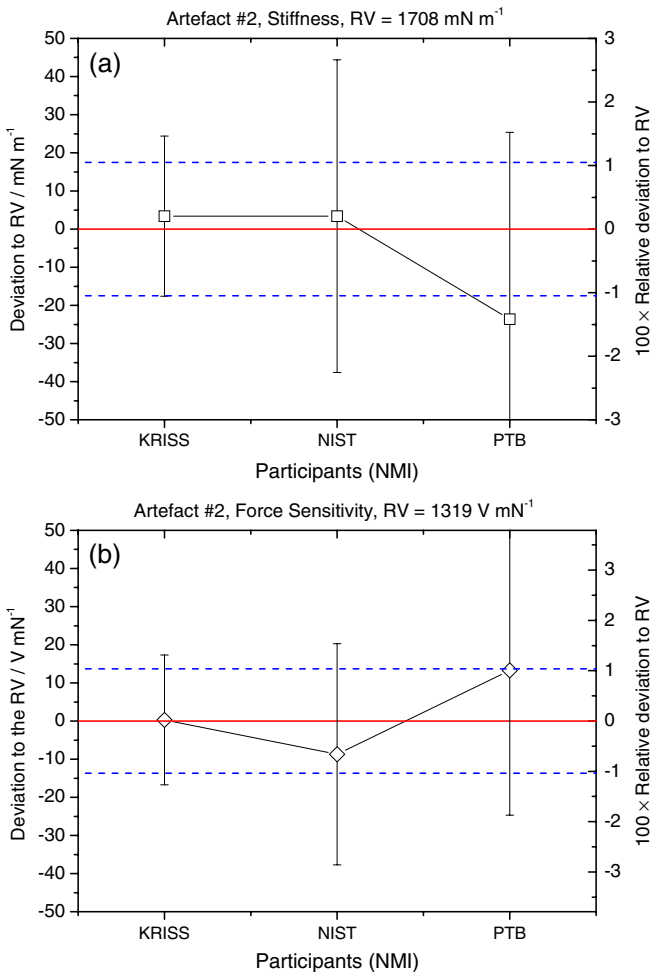


**Figure A2.** Comparison results for (*a*) the stiffness and (*b*) the force sensitivity of artefact #2 after subtraction of the RVs: (*a*) 1708 mN m$^{-1}$ and (*b*) 1319 V mN$^{-1}$ calculated from the weighted mean values of the measurement data. Dashed blue lines represent the expanded uncertainties of the RVs. Note that all reported mean values are within the uncertainty bounds of RVs (error bars are described in the text).

## Acknowledgments

M-S Kim is grateful to the Korea Research Foundation Grant Program funded by the Korean Government (MOEHRD) (KRF-2007-611-D00010) and to the NIST Mass and Force group for support during his stay at NIST. J R Pratt acknowledges the support of his colleagues in the Mass and Force Group and the technical contributions of John Kramar, who assisted with data analysis. NPL's participation was funded by the UK NMO Engineering Measurement Programme. C W Jones acknowledges the support of NPL colleague Richard Leach.

## Appendix. Comparison results of artefacts #1 and #2

Additional transfer artefacts numbered 1 and 2 of the FMT-400 model were calibrated by KRISS, NIST and PTB and the results for artefacts #1 and #2 were compared and are shown in figures A1 and A2, respectively.

## References

[1] Choi J H 2010 Measurement, back-action and future standard in ultra-small force metrology, http://www.imeko.org/publications/tc3-2010/IMEKO-TC3-2010-WS-005.pdf (accessed: 15 March 2011)
[2] Jones C W 2010 Low force metrology at the National Physical Laboratory, UK, http://www.imeko.org/publications/tc3-2010/IMEKO-TC3-2010-WS-002.pdf (accessed: 15 March 2011)
[3] Kim M S 2010 Current status and perspective on low force metrology in Korea, http://www.imeko.org/publications/tc3-2010/IMEKO-TC3-2010-WS-003.pdf (accessed: 15 March 2011)
[4] Menelao F 2010 Micro and Nanoforce metrology at PTB, http://www.imeko.org/publications/tc3-2010/IMEKO-TC3-2010-WS-001.pdf (accessed: 15 March 2011)
[5] Pratt J R 2006 The small force metrology laboratory at the National Institute of Standards and Technology, http://www.imeko.org/publications/wc-2006/PWC-2006-RT-TC3-002u.ppt (accessed: 15 March 2011)
[6] Pan S S 2010 The activities of micro force measurement below 10 mN in Center for Measurement Standards, http://www.imeko.org/publications/tc3-2010/IMEKO-TC3-2010-WS-004.pdf (accessed: 15 March 2011)
[7] Kim M S, Choi J H, Park Y K and Kim J H 2006 Atomic force microscope cantilever calibration device for quantified force metrology at micro- or nano-scale regime: the nano force calibrator (NFC) *Metrologia* **43** 389–95
[8] Leach R, Chetwynd D, Blunt L, Haycocks J, Harris P, Jackson K, Oldfield S and Reilly S 2006 Recent advances in traceable nanoscale dimension and force metrology in the UK *Meas. Sci. Technol.* **17** 467–76
[9] Nesterov V 2007 Facility and methods for the measurement of micro and nano forces in the range below $10^{-5}$ N with a resolution of $10^{-12}$ N (development concept) *Meas. Sci. Technol.* **18** 360–6
[10] Pratt J R, Kramar J A, Newell D B and Smith D T 2005 Review of SI traceable force metrology for instrumented indentation and atomic force microscopy *Meas. Sci. Technol.* **16** 2129–37
[11] Doering L and Brand U 2006 Calibration of V-shaped cantilever for micro force metrology in biomedical engineering *Proc. 6th Euspen Int. Conf.* (*Baden bei Wien, Austria*, *28 May–1 June 2006*) pp 192–5
[12] Kim M S, Choi J H, Kim J H and Park Y K 2007 SI-traceable determination of spring constants of various atomic force microscope cantilevers with a small uncertainty of 1% *Meas. Sci. Technol.* **18** 3351–8
[13] Cumpson P J, Clifford C A and Hedley J 2004 Quantitative analytical atomic force microscopy: a cantilever reference device for easy and accurate AFM spring-constant calibration *Meas. Sci. Technol.* **15** 1337–46
[14] Cumpson P J and Hedley J 2003 Accurate analytical measurements in the atomic force microscope: a microfabricated spring constant standard potentially traceable to the SI *Nanotechnology* **14** 1279–88
[15] Cumpson P J, Hedley J and Zhdan P 2003 Accurate force measurement in the atomic force microscope: a microfabricated array of reference springs for easy cantilever calibration *Nanotechnology* **14** 918–24
[16] Gates R S and Pratt J R 2006 Prototype cantilevers for SI-traceable nanonewton force calibration *Meas. Sci. Technol.* **17** 2852–60
[17] Gates R S and Reitsma M G 2007 Precise atomic force microscope cantilever spring constant calibration using a reference cantilever array *Rev. Sci. Instrum.* **78** 086101
[18] Langlois E D, Shaw G A, Kramar J A, Pratt J R and Hurley D C 2007 Spring constant calibration of atomic

force microscopy cantilevers with a piezosensor transfer standard *Rev. Sci. Instrum.* **78** 093705
[19] Behrens I, Doering L and Peiner E 2003 Piezoresistive cantilever as portable micro force calibration standard *J. Micromech. Microeng.* **13** S171–7
[20] Chung K H, Scholz S, Shaw G A, Kramar J A and Pratt J R 2008 SI traceable calibration of an instrumented indentation sensor spring constant using electrostatic force *Rev. Sci. Instrum.* **79** 095105
[21] Chung K H, Pratt J R and Reitsma M G 2010 Lateral force calibration: accurate procedures for colloidal probe friction measurements in atomic force microscopy *Langmuir* **26** 1386–94
[22] Chung K H, Shaw G A and Pratt J R 2009 Accurate noncontact calibration of colloidal probe sensitivities in atomic force microscopy *Rev. Sci. Instrum.* **80** 065107
[23] Kim M S, Choi J H, Kim J H and Park Y K 2010 Accurate determination of spring constant of atomic force microscope cantilevers and comparison with other methods *Measurement* **43** 520–6
[24] Pratt J R, Shaw G A, Kumanchik L and Burnham N A 2010 Quantitative assessment of sample stiffness and sliding friction from force curves in atomic force microscopy *J. Appl. Phys.* **107** 044305
[25] Matei G A, Thoreson E J, Pratt J R, Newell D B and Burnham N A 2006 Precision and accuracy of thermal calibration of atomic force microscopy cantilevers *Rev. Sci. Instrum.* **77** 083703
[26] ISO 376 2011 *Metallic Materials—Calibration of Force-Proving Instruments used for the Verification of Uniaxial Testing Machines* 4th edn (Geneva: International Standards Organization)
[27] Kim M S and Pratt J R 2010 SI traceability: current status and future trends for forces below 10 microNewtons *Measurement* **43** 169–82
[28] Leach R, Oldfield S and Georgakopoulos D 2006 Traceable nanonewton force measurement at the National Physical Laboratory *Proc. 6th Euspen Int. Conf.* (*Baden bei Wien, Austria*, *28 May–1 June 2006*) pp 414–7
[29] Jones C W and Leach R K 2008 Review of low force transfer artefact technologies *NPL Report Eng 5* (Teddington, UK: National Physical Laboratory)
[30] Klocke Nanotechnik: Force Feedback Systems, http://www.nanomotor.de/n_force_feedback.htm (accessed: 20 December 2008)
[31] Edwards S A, Ducker W A and Sader J E 2008 Influence of atomic force microscope cantilever tilt and induced torque on force measurements *J. Appl. Phys.* **103** 064513
[32] BIPM, IEC, IFCC, ISO, IUPAC, IUPAP and OIML 1995 *Guide to the Expression of Uncertainty in Measurement* 2nd edn (Geneva: International Standards Organization)